LETTERS
PUBLISHED ONLINE: 28 APRIL 2014 | DOI: 10.1038/NNANO.2014.81
nature nanotechnology

Flexible metallic nanowires with self-adaptive contacts to semiconducting transition-metal dichalcogenide monolayers

Junhao Lin[1,2†*], Ovidiu Cretu[3†], Wu Zhou[2*], Kazu Suenaga[3], Dhiraj Prasai[4], Kirill I. Bolotin[1], Nguyen Thanh Cuong[3], Minoru Otani[3], Susumu Okada[5], Andrew R. Lupini[2], Juan-Carlos Idrobo[6], Dave Caudel[1,7], Arnold Burger[7], Nirmal J. Ghimire[2,8], Jiaqiang Yan[2,9], David G. Mandrus[2,8,9], Stephen J. Pennycook[9] and Sokrates T. Pantelides[1,2]

In the pursuit of ultrasmall electronic components[1–5], monolayer electronic devices have recently been fabricated using transition-metal dichalcogenides[6–8]. Monolayers of these materials are semiconducting, but nanowires with stoichiometry MX (M = Mo or W, X = S or Se) have been predicted to be metallic[9,10]. Such nanowires have been chemically synthesized[11–13]. However, the controlled connection of individual nanowires to monolayers, an important step in creating a two-dimensional integrated circuit, has so far remained elusive. In this work, by steering a focused electron beam, we directly fabricate MX nanowires that are less than a nanometre in width and Y junctions that connect designated points within a transition-metal dichalcogenide monolayer. *In situ* electrical measurements demonstrate that these nanowires are metallic, so they may serve as interconnects in future flexible nanocircuits fabricated entirely from the same monolayer. Sequential atom-resolved Z-contrast images reveal that the nanowires rotate and flex continuously under momentum transfer from the electron beam, while maintaining their structural integrity. They therefore exhibit self-adaptive connections to the monolayer from which they are sculpted. We find that the nanowires remain conductive while undergoing severe mechanical deformations, thus showing promise for mechanically robust flexible electronics. Density functional theory calculations further confirm the metallicity of the nanowires and account for their beam-induced mechanical behaviour. These results show that direct patterning of one-dimensional conducting nanowires in two-dimensional semiconducting materials with nanometre precision is possible using electron-beam-based techniques.

Previous work has reported the fabrication of nanoribbons in a MoS_2 monolayer using the electron beam from a transmission electron microscope (TEM)[14]. These nanoribbons were determined, via image simulations and theory, to have Mo_5S_4 stoichiometry and then predicted to be semiconducting[14]. Such top-down fabrication of nanostructures within a monolayer shows that electron-beam engineering of the atomic structure of a two-dimensional material is achievable on the nanometre scale. Here, we will show that the focused electron beam of a scanning TEM (STEM) provides precise and flexible control over the illumination regions where the electrons interact with the sample. We will demonstrate that nanowires fabricated in transition-metal dichalcogenide (TMDC) monolayers using an electron beam have the same MX stoichiometry in their final stable forms and are in fact metallic, as required for applications in nanoelectronics.

To fabricate nanowires at designated positions with nanometre-scale precision we make use of ionization etching[15] of semiconducting TMDC monolayers under a focused low-energy electron beam (typically 60 kV, see Methods) in a STEM. Figure 1a presents a Z-contrast (Z is the atomic number) image of the controlled patterning of a nanowire network fabricated directly from a $MoSe_2$ monolayer (Supplementary Fig. 1). The central small $MoSe_2$ patch is connected to the parent monolayer by several nanowires with the same crystal structure.

Supplementary Fig. 2 presents a detailed schematic of our fabrication process for an individual nanowire with location control. Prolonged exposure of TMDC monolayers to a 60 kV electron beam generates vacancies and vacancy complexes[16] that can expand into relatively large holes in the scanned regions, primarily due to the ionization effect[16–18] (see Supplementary Section 3 for a detailed discussion). By focusing the electron beam at selected regions, two holes were drilled side by side, thereby confining a ribbon of the monolayer at the designated site (Supplementary Fig. 3b). Further electron irradiation changed such ribbons of monolayers into thick wires (Fig. 1c,h) due to the redeposition of atoms that had been etched away from the edges of the ribbons. Figure 1e–g and i–l show a few STEM Z-contrast images extracted from Supplementary Movies 1 and 2, demonstrating the thinning of these thick wires by either etching away excess atoms from the thick structure (Supplementary Movie 1) with the electron beam or unzipping from the centre of the thick wire, with the excess atoms diffusing away to the end junctions (Supplementary Movie 2). When the wire has narrowed to a critical width of ~5 Å, the centre section self-assembles into a stable nanowire structure, as shown in Fig. 1e,j. Figure 1g,l shows the final results of sculpting an individual nanowire within the scanning window of the electron beam. No significant amount of carbon is

[1]Department of Physics and Astronomy, Vanderbilt University, Nashville, Tennessee 37235, USA, [2]Materials Science & Technology Division, Oak Ridge National Laboratory, Oak Ridge, Tennessee 37831, USA, [3]National Institute of Advanced Industrial Science and Technology (AIST), Tsukuba 305-8565, Japan, [4]Interdisciplinary Graduate Program in Materials Science, Vanderbilt University, Nashville, Tennessee 37235, USA, [5]Graduate School of Pure and Applied Sciences, University of Tsukuba, Tsukuba 305-8571, Japan, [6]Center for Nanophase Materials Sciences, Oak Ridge National Laboratory, Oak Ridge, Tennessee 37831, USA, [7]Department of Physics, Fisk University, Nashville, Tennessee 37208, USA, [8]Department of Physics and Astronomy, University of Tennessee, Knoxville, Tennessee 37996, USA, [9]Department of Materials Science and Engineering, University of Tennessee, Knoxville, Tennessee 37996, USA. [†]These authors contributed equally to this work. *e-mail: junhao.lin@vanderbilt.edu; wu.zhou.stem@gmail.com

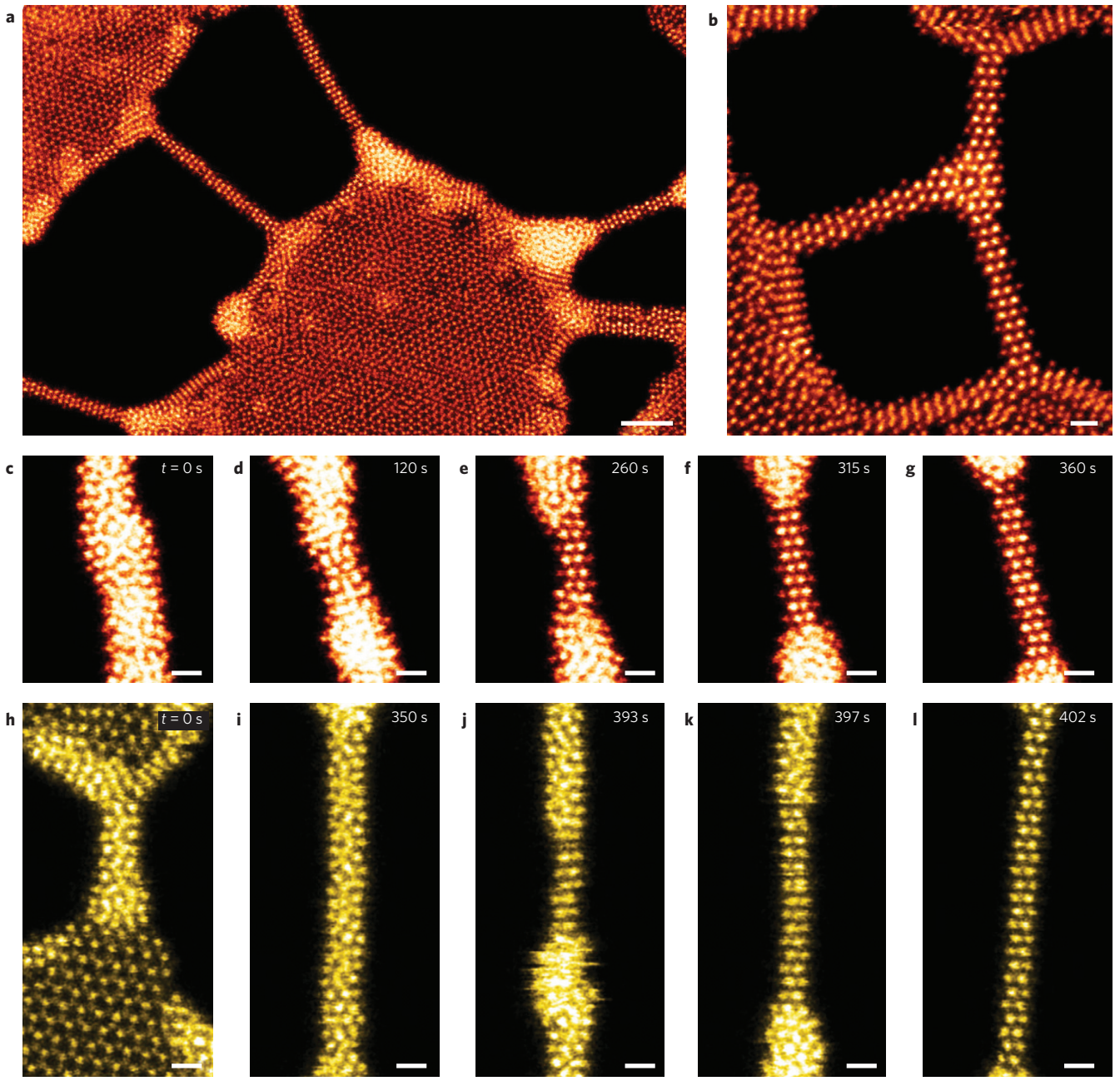

Figure 1 | Fabrication of nanowires from TMDC monolayers using a focused electron beam. a, Patterning of a MoSe nanowire network, where each nanowire is sculpted individually. **b**, A ramified Y junction made of three MoSe nanowires. **c**–**l**, Serial snapshots of the sculpting process of individual MoSe (**c**–**g**) and MoS (**h**–**l**) nanowires. All images are STEM Z-contrast images, false-coloured for better visibility. Scale bars, 2 nm (**a**), 0.5 nm (**b**–**l**).

incorporated into the wire during this fabrication process (Supplementary Fig. 4; see Methods).

We have also controllably fabricated nanowires in other semiconducting TMDC monolayers, such as WSe_2 (Supplementary Fig. 5, Supplementary Movie 3). The spatial precision for positioning the nanowire using our method is on the nanometre scale (<5 nm in the transverse direction of the nanowire), which is mainly determined by the separation of the two patterned holes in the TMDC layer.

The length of the nanowire can be controlled by adjusting the size of the holes that confine the monolayer ribbons. We have succeeded in fabricating nanowires as long as ~10 nm. It is important to note that, during fabrication, different initial structures always reconstruct into the same final stable nanowire (Fig. 1e,j); that is, the fabrication process is self-regulating, possibly driven by spontaneous phase transition[14]. Meanwhile, these as-formed nanowires are highly robust against direct knock-on damage from the electron beam, as the threshold for knocking out atoms from the nanowires is much higher than 60 kV (Supplementary Tables 1 and 2). Occasionally, we observe that the capping S or Se atoms of the nanowire are removed by the electron beam, but recapping occurs rapidly via atomic diffusion (Supplementary Movie 4) because of the low diffusion barrier (Supplementary Fig. 14). These processes impart self-healing characteristics to the nanowires, allowing for simultaneous fabrication of multiple nanowires by drilling multiple holes side by side. To connect three (or more) nanowires to create junctions, we patterned the holes in a triangular shape and exposed the confined ribbons alternately to the electron beam (Supplementary Fig. 6). A ramified Y junction connecting three MoSe nanowires is shown in Fig. 1b, demonstrating the

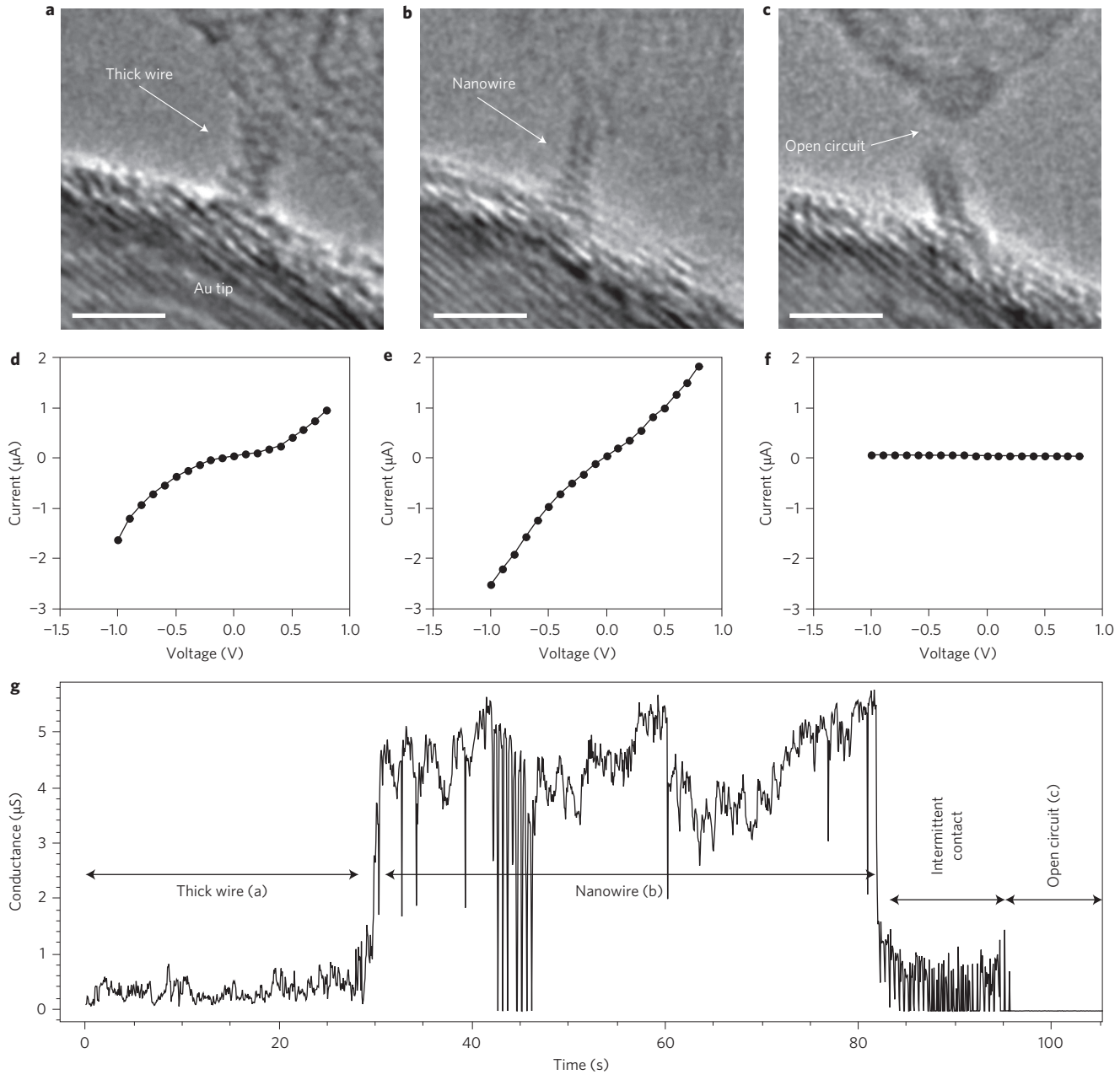

Figure 2 | *In situ* electrical measurement of a MoSe nanowire. a–c, TEM images acquired during *in situ* fabrication of a MoSe nanowire between a gold contact and layered $MoSe_2$, showing the initial formation of the MoSe thick wire (**a**, similar to Fig. 1c), formation of the stable MoSe nanowire (**b**) and breaking of the nanowire (**c**). **d–f**, Current–voltage measurements corresponding to **a–c**, respectively. **g**, Time evolution of conductance during the formation and breaking of another MoSe nanowire (also shown in Supplementary Movie 5). Labels (a) to (c) for different periods in the figure refer to generic stages of formation/destruction of a nanowire, similar to those shown in **a–c**. The voltage is kept constant at 1 V (ref. 6). Noise is due to mechanical instabilities of the experimental set-up. The TEM images have been processed with a band-pass filter. Scale bars, 2 nm.

diversity of the building blocks that can be fabricated by steering the focused electron beam of the STEM. In contrast, control over the location of the nanowires and fabrication of such junctions would not be practical using the TEM-based technique reported in ref. 14.

As the formation of the nanowire is self-regulating under electron irradiation, we were able to fabricate the same MoSe nanowires using a TEM (Supplementary Fig. 7) that is capable of *in situ* electrical measurements (see Methods for details). We performed current–voltage measurements at various stages during *in situ* fabrication of the MoSe nanowire. The results are summarized in Fig. 2, where the $MoSe_2$ layer is seen to first form a thick wire (Fig. 2a, similar to the structure characterized in the STEM and shown in Fig. 1c) and subsequently forms a stable MoSe nanowire structure (Fig. 2b). The corresponding electrical data (Fig. 2d,e) show a substantial increase in electrical conductance as the nanowire forms, direct evidence of the conversion of the semiconducting monolayer to a metallic nanowire. The time evolution of the conductance during *in situ* fabrication of another individual MoSe nanowire is plotted in Fig. 2g. Supplementary Movie 5 shows this formation process, correlated with a dynamic version of the plot. The formation of the nanowire marks an ~15-fold increase in electrical conductance (estimated from the mean values before and after formation of the nanowire), which remained roughly the same throughout the lifetime of the nanowire. Furthermore, the metallic

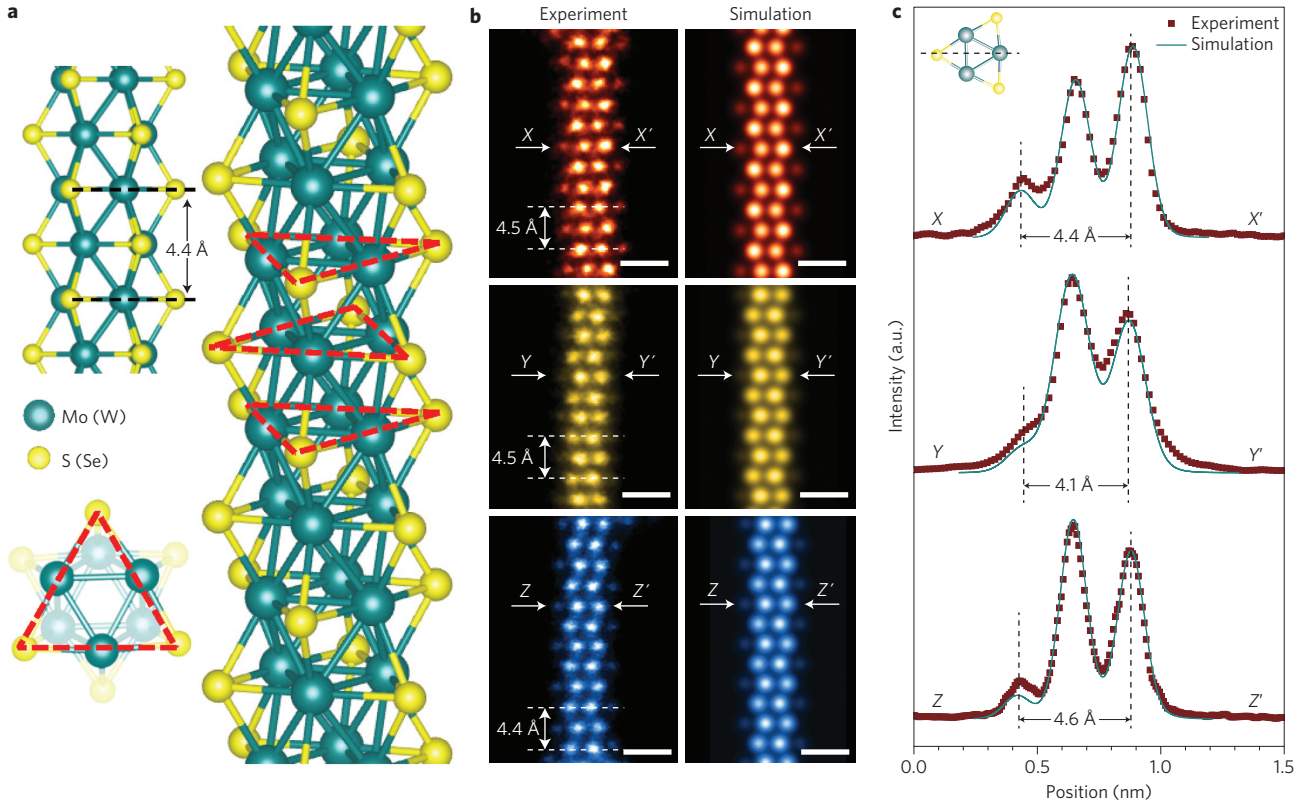

Figure 3 | Atomic structure of the nanowire. a, Atomic structural model of the nanowires. Dashed red triangles indicate the orientation of each layer in the nanowire. **b**, Experimental (left) and simulated (right) STEM Z-contrast images of individual MoSe (orange), MoS (yellow) and WSe (blue) nanowires. The axial lattice constant is measured from the experimental images. **c**, Normalized intensity line profile along the *X*–*X*′, *Y*–*Y*′ and *Z*–*Z*′ directions in **b**, with a side view of the atomic structural model provided in the inset. Scale bars, 0.5 nm.

nature of the nanowires is consistent with the fact that they are much more stable under the electron beam than their parent semiconducting TMDC monolayers.

The nonlinear *I*–*V* curves (Fig. 2d,e) suggest a Schottky-like contact, which may occur at connections between the nanowire, the $MoSe_2$ layers and/or the gold tip. In addition, we found that the gold tip is sometimes covered by a few layers of amorphous material (either carbon or Mo_xSe_y from previous experiments), leading to a slightly lower conductance (~5 μS, as compared to ballistic conductance in a one-dimensional system[5]). The mechanical instability of the contact between the gold tip and the nanowire also leads to fluctuations in the measured electrical conductance (the fluctuation is about ±19%), as the contact resistance varies when the contact geometry changes (Supplementary Movie 5). On the other hand, theoretical calculations (Supplementary Figs 15 and 16) suggest that as-fabricated contacts between nanowires and the parent monolayer are ohmic if the monolayer is doped p-type. It may be possible to achieve such contacts in the future when interconnects between devices are fabricated directly by electron beams.

To understand the observed metallicity of the nanowires, we performed density functional theory (DFT) calculations based on the STEM Z-contrast images shown in Fig. 1, enabling us to visualize every atom in the stable nanowires and identify their precise configuration. Figure 3a presents the atomic structure of the nanowires, with 1:1 atomic ratio of Mo (W) and S (Se). The Mo (W) and S (Se) atoms in the nanowires are arranged in consecutive stacks of triangular layers rotated 180° along the nanowire axial direction, with three capping S (Se) atoms located at the vertices of the triangles and three Mo (W) atoms located between the S (Se) atoms. Figure 3b,c compares the experimental STEM images of MoSe, MoS and WSe nanowires with simulated images using the atomic model in Fig. 3a, showing an excellent match at all atomic positions. The measured axial lattice constants are also in good agreement with the DFT calculations (Supplementary Fig. 8). The width of the conducting nanowire is measured to be 4.4 Å for MoSe, 4.1 Å for MoS and 4.6 Å for WSe, an ultrasmall diameter comparable to that of the smallest carbon nanotubes (4 Å)[2]. DFT calculations show that the metallic characteristics of this nanowire family are a result of the strong hybridization between the *d* orbitals of the transition-metal atoms with the *p* orbitals of the chalcogen atoms (S or Se), which form free electron-like bands crossing the Fermi level (Supplementary Fig. 9)[9,10].

It should be pointed out that the above MX nanowire structure was predicted by theory to be energetically more stable than other alternative structures[10], including the Mo_5S_4 structure reported in ref. 14. Furthermore, high-resolution TEM (HRTEM) image simulation based on the MoS nanowire structure reproduces well the experimental images reported in ref. 14 (see Supplementary Fig. 13 for details), suggesting that the 'nanoribbons' of ref. 14 have the same MX structure and are indeed metallic.

We further explored the mechanical flexibility of the nanowires via sequential imaging, where the electron beam acts as a source to excite deformations of the nanowire. We found that the nanowires can rotate, flex and bend continuously under electron irradiation, while maintaining their stable atomic structure, a strong indication of excellent mechanical flexibility (Supplementary Movies 1–3, 6). Bending of the nanowires is demonstrated in Fig. 4d,e, which is recoverable, as shown in Supplementary Movie 6, consistent with previous theoretical studies[19]. Figure 4a–c provides an atomic-scale analysis of the rotation and out-of-plane deflection of the nanowires. The

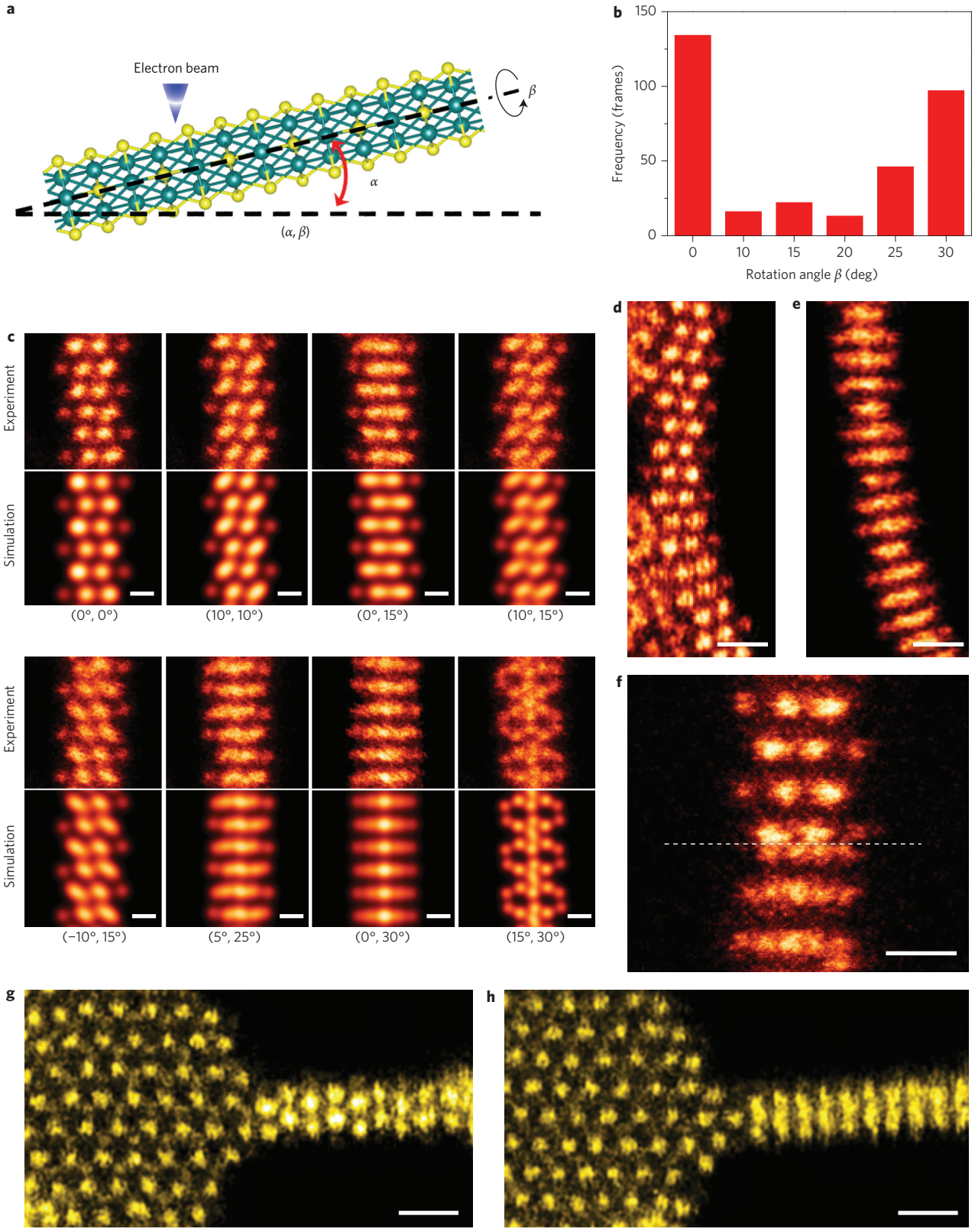

Figure 4 | Flexing and discrete rotations of a nanowire between junctions. a, Schematic of dynamic movements of the nanowire. α is the out-of-plane deflection angle of the nanowire and β is the rotation angle along the *c* axis of the nanowire. **b**, Statistics of different rotation angles observed on a MoSe nanowire during sequential STEM imaging. **c**, Experimental and simulated STEM images showing different combinations of rotation and deflection of the MoSe nanowire. **d**,**e**, Experimental STEM images showing bending of MoSe nanowires. **f**, STEM image showing the fast switching of a MoSe nanowire between discrete rotations. The white dashed line indicates the boundary between two different rotation states. **g**,**h**, STEM images of the atomic junction between MoS nanowires and MoS_2 monolayers in different configurations. The nanowire rotates 30° along the *c* axis of the nanowire between the two images, and the junction reconstructs accordingly. Scale bars, 0.2 nm (**c**), 0.5 nm (**d**,**e**), 0.2 nm (**f**), 0.5 nm (**g**,**h**).

atomic-scale rotations occur at several discrete stable rotation angles, with rapid switching between them. Figure 4a presents a schematic diagram of out-of-plane deflection and rotation along the *c* axis of the nanowires, with the angles indicated by (α, β), respectively. A set of discrete stable rotation states, indicated by the corresponding (α, β) of the nanowire observed during the sequential imaging, are shown in Fig. 4c. A maximum out-of-plane deflection angle of ~15° was observed. Rotations up to 30° can be identified, with ~5° accuracy. The 0° and 30° rotation states are much more stable than others, as shown by the histogram in Fig. 4b.

The rotation of the nanowires by discrete angles is further demonstrated in Fig. 4f, where the whole nanowire rotates 30° while the electron beam is scanning across one atomic layer of the nanowire, as indicated by the dashed line. The fast switching between specific rotation angles is estimated to be in the millisecond range (see Methods) and was consistently observed under different scanning settings (Supplementary Fig. 10).

The fact that the nanowires can rotate through a large angle without being torn apart suggests that the rotations are accompanied by self-adaptive reconstruction at the atomic junctions between the nanowires and the TMDC monolayers. Figure 4g,h shows two stable configurations of the atom-wide junctions, differing by a 30° rotation of the nanowire. After rotation, the nanowire reconnects seamlessly to the MoS_2 monolayer; that is, the junction is self-adaptive (Supplementary Fig. 11). The nanowire–monolayer junctions generally form and persistently reconstruct at protrusions of the monolayer edges, with minimum bonding constraints from neighbouring atoms. Such a pivot-like junction structure enables the nanowire to switch between different rotation angles with minimum energy. DFT calculations based on a shorter nanowire (Supplementary Fig. 12) account for the most stable 0° and 30° rotation states observed experimentally (Fig. 4b), and find a maximum energy barrier of ~3 eV for the whole nanowire to rotate, which can be overcome easily with the energy transferred from the electron beam[20].

Combining the *in situ* time-evolved conductance measurements (Fig. 2g, Supplementary Movie 5) and the mechanical flexibility of the nanowire (Fig. 4), we have shown that the nanowire remains conductive when it undergoes mechanical deformation (rotations and flexing). This result confirms that the self-adaptive nature of the nanowire–monolayer junction does not change the electronic properties of either the nanowire or the junction, as further confirmed by DFT calculations (Supplementary Figs 15 and 16). This will be important for future flexible nanoelectronics.

TMDC-based devices with excellent mechanical flexibility have inspired research on assembling multiple devices into circuits[21,22]. The pliable metallic nanowires described in this Letter, with robust junctions at designated locations, may serve to connect multiple atom-thick nanoelectronic components with a view to creating two-dimensional fully integrated flexible nanocircuits. Moreover, together with the pioneering results from ref. 14, the formation of these nanowires can be achieved with various acceleration voltage and vacuum levels (see Methods), suggesting it may be possible in the future to first fabricate devices in a TDMC monolayer and subsequently sculpt high-quality nanowire interconnects using a scanning electron microscope or an electron-beam lithography system with optimized fabrication parameters, such as precise dose control of electron irradiation. Furthermore, production could be scalable, because it is insensitive to the initial shape of the monolayer, all nanowires eventually collapse to their stable structures, and the nanowires are self-healing under electron beam irradiation. The smallest separation between the nanowires depends on how close the holes can be patterned, which should be achievable in the sub-100 nm regime. Combined with the self-adaptive contacts to the TMDC monolayer, which accommodate the mechanical behaviour of the nanowire, these ultra-flexible sub-nanometre-wide conducting nanowires could serve as robust one-dimensional electron channels and provide a new building block for future flexible integrated nanoelectronics[23].

Methods

Sample preparation. MoS_2, $MoSe_2$ and WSe_2 monolayer samples were exfoliated from bulk crystals. Similar to exfoliating monolayer graphene, we mechanically exfoliated the bulk material onto a Si wafer coated with 300 nm SiO_2 using the scotch-tape method and identified the monolayers under an optical microscope[24]. We then transferred the monolayer flakes to TEM grids, based on a polymer-free method[25], for nanowire fabrication. Extra care was taken throughout sample preparation and microscopy experiments to avoid carbon contamination. This included storing the samples under vacuum and performing ion cleaning on the Au tips before each *in situ* experiment. Moreover, our experiments were performed on carefully selected clean regions of monolayers, which did not show noticeable contaminations in Z-contrast images.

***In situ* fabrication and imaging of nanowires.** Fabrication of the nanowires was performed on a Nion UltraSTEM-100 operating at 60 kV (ref. 26) under ultrahigh vacuum (~1×10^{-9} torr). This fabrication process can also be realized at 100 kV, but with less control on patterning of the holes. The adjustable beam current (up to ~100 pA) was used to control the sculpting process of the nanowires. The converged electron beam could be controlled to scan selected regions. The dwell time per pixel was set to 2–4 μs (with repeated scans) for sculpting of the nanowire and 16–24 μs for imaging. Supplementary Movies 1, 2, 4 and 6 are played at 5 times the recorded rate, and Supplementary Movie 3 is played at 3 times the recorded rate. All Z-contrast images were low-pass-filtered to reduce random noise.

Experimental set-up for *in situ* electrical measurement of the nanowire. Fabrication of nanowires for *in situ* electrical measurements was performed on a JEOL 2010F TEM under a vacuum of ~1×10^{-7} torr. $MoSe_2$ crystals were exfoliated using micromechanical cleavage. Some flakes were subsequently transferred to a dedicated sample holder[27], where the exposed flakes at the edge could be contacted with a gold tip prepared by electrochemical etching[28]. A source meter connected to both sample and tip was used to collect the electrical data. To fabricate the nanowire, a few-layer region located at the end of a $MoSe_2$ flake was contacted with the gold tip. An electrical bias of the order of 2 V was then applied, leading to joule heating (electrical annealing) of the region around the contact. Electron irradiation from the 120 kV electron beam led to gradual thinning of the area and formation of the nanowire, similar to the fabrication process in the STEM. The bias was lowered to ~1 V and kept fixed during the final stages, allowing more control over the process. The time-evolved conductance was derived from the electrical current, which was constantly recorded throughout the fabrication. The bias was interrupted over short periods of time (~1 s), to allow the acquisition of *I*–*V* measurements at different stages of fabrication.

Estimating the rotation angle of the nanowires. The rotation and out-of-plane deflection angles of the experimental images in Fig. 4 were estimated by comparing experimental and simulated images, using 5° per step as it is difficult to distinguish small rotations of the nanowires from the images. Moreover, the rotation angle of 5° cannot be distinguished from 0°, because the difference of projected atomic positions between these two rotation angles is too small to be resolved. Due to the three-fold symmetry of the nanowire, the rotation was antisymmetrical at 60°. However, the experimental images of 0° and 60° rotations look practically identical due to the growth of the nanowire and possible image drift between successive frames. Therefore, in our statistical study (Fig. 4b) the rotation angle is only identified from 0° to 30°.

Received 14 October 2013; accepted 20 March 2014; published online 28 April 2014

References

1. Kondo, Y. & Takayanagi, K. Synthesis and characterization of helical multi-shell gold nanowires. *Science* **289,** 606–608 (2000).
2. Qin, L. C. *et al.* Materials science—the smallest carbon nanotube. *Nature* **408,** 50 (2000).
3. Xiang, J. *et al.* Ge/Si nanowire heterostructures as high-performance field-effect transistors. *Nature* **441,** 489–493 (2006).
4. Yanson, A. I., Bollinger, G. R., van den Brom, H. E., Agrait, N. & van Ruitenbeek, J. M. Formation and manipulation of a metallic wire of single gold atoms. *Nature* **395,** 783–785 (1998).
5. Ohnishi, H., Kondo, Y. & Takayanagi, K. Quantized conductance through individual rows of suspended gold atoms. *Nature* **395,** 780–783 (1998).
6. Radisavljevic, B., Radenovic, A., Brivio, J., Giacometti, V. & Kis, A. Single-layer MoS_2 transistors. *Nature Nanotech.* **6,** 147–150 (2011).
7. Wang, Q. H., Kalantar-Zadeh, K., Kis, A., Coleman, J. N. & Strano, M. S. Electronics and optoelectronics of two-dimensional transition metal dichalcogenides. *Nature Nanotech.* **7,** 699–712 (2012).

8. Yin, Z. *et al.* Single-layer MoS_2 phototransistors. *ACS Nano* **6,** 74–80 (2012).
9. Cakir, D., Durgun, E., Gulseren, O. & Ciraci, S. First principles study of electronic and mechanical properties of molybdenum selenide type nanowires. *Phys. Rev. B* **74,** 235433 (2006).
10. Murugan, P., Kumar, V., Kawazoe, Y. & Ota, N. Assembling nanowires from Mo–S clusters and effects of iodine doping on electronic structure. *Nano Lett.* **7,** 2214–2219 (2007).
11. Kibsgaard, J. *et al.* Atomic-scale structure of Mo_6S_6 nanowires. *Nano Lett.* **8,** 3928–3931 (2008).
12. Venkataraman, L., Hong, Y. S. & Kim, P. Electron transport in a multichannel one-dimensional conductor: molybdenum selenide nanowires. *Phys. Rev. Lett.* **96,** 076601 (2006).
13. Venkataraman, L. & Lieber, C. M. Molybdenum selenide molecular wires as one-dimensional conductors. *Phys. Rev. Lett.* **83,** 5334–5337 (1999).
14. Liu, X. *et al.* Top down fabrication of sub-nanometre semiconducting nanoribbons derived from molybdenum disulfide sheets. *Nature Commun.* **4,** 1776 (2013).
15. Egerton, R. F., Li, P. & Malac, M. Radiation damage in the TEM and SEM. *Micron* **35,** 399–409 (2004).
16. Zhou, W. *et al.* Intrinsic structural defects in monolayer molybdenum disulfide. *Nano Lett.* **13,** 2615–2522 (2013).
17. Zan, R. *et al.* Control of radiation damage in MoS_2 by graphene encapsulation. *ACS Nano* **7,** 10167–10174 (2013).
18. Komsa, H-P. *et al.* Two-dimensional transition metal dichalcogenides under electron irradiation: defect production and doping. *Phys. Rev. Lett.* **109,** 035503 (2012).
19. Popov, I., Gemming, S., Okano, S., Ranjan, N. & Seifert, G. Electromechanical switch based on Mo_6S_6 nanowires. *Nano Lett.* **8,** 4093–4097 (2008).
20. Lee, J., Zhou, W., Pennycook, S. J., Idrobo, J-C. & Pantelides, S. T. Direct visualization of reversible dynamics in a Si_6 cluster embedded in a graphene pore. *Nature Commun.* **4,** 1650 (2013).
21. Radisavljevic, B., Whitwick, M. B. & Kis, A. Integrated circuits and logic operations based on single-layer MoS_2. *ACS Nano* **5,** 9934–9938 (2011).
22. Wang, H. *et al.* Integrated circuits based on bilayer MoS_2 transistors. *Nano Lett.* **12,** 4674–4680 (2012).
23. Chau, R., Doyle, B., Datta, S., Kavalieros, J. & Zhang, K. Integrated nanoelectronics for the future. *Nature Mater.* **6,** 810–812 (2007).
24. Novoselov, K. S. *et al.* Electric field effect in atomically thin carbon films. *Science* **306,** 666–669 (2004).
25. Regan, W. *et al.* A direct transfer of layer-area graphene. *Appl. Phys. Lett.* **96,** 113102 (2010).
26. Krivanek, O. L. *et al.* An electron microscope for the aberration-corrected era. *Ultramicroscopy* **108,** 179–195 (2008).
27. Svensson, K., Jompol, Y., Olin, H. & Olsson, E. Compact design of a transmission electron microscope-scanning tunneling microscope holder with three-dimensional coarse motion. *Rev. Sci. Instrum.* **74,** 4945–4947 (2003).
28. Ren, B., Picardi, G. & Pettinger, B. Preparation of gold tips suitable for tip-enhanced Raman spectroscopy and light emission by electrochemical etching. *Rev. Sci. Instrum.* **75,** 837–841 (2004).

Acknowledgements

The authors thank H. Conley for helping with the transfer of the samples, E. Rowe, E. Tupitsyn and P. Bhattacharya for early technical assistance on the samples, and R. Ishikawa, R. Mishra, B. Wang and J. Lou for discussions. This research was supported in part by the US Department of Energy (DOE; grant DE-FG02-09ER46554 to J.L. and S.T.P.), a Wigner Fellowship through the Laboratory Directed Research and Development Program of Oak Ridge National Laboratory (ORNL), managed by UT-Battelle, LLC, for the US DOE (W.Z.), the Office of Basic Energy Sciences, Materials Sciences and Engineering Division, US DOE (A.R.L., N.J.G., J.Q.Y., D.G.M., S.J.P. and S.T.P.) and through a user project supported by ORNL's Center for Nanophase Materials Sciences (CNMS), which is sponsored by the Scientific User Facilities Division, Office of Basic Energy Sciences, US DOE (J.C.I.). K.I.B. and D.P. were supported by ONR N000141310299. This research used resources of the National Energy Research Scientific Computing Center, which is supported by the Office of Science of the US DOE (contract no. DE-AC02-05CH11231). O.C. and K.S. acknowledge the Japan Science and Technology Agency (JST) research acceleration programme for financial support. N.T.C., M.O. and S.O. acknowledge support from the JST-CREST programme.

Author contributions

J.L. and O.C. designed and carried out the experiments and analysed the data. J.L. performed the STEM experiments and first-principles calculations. O.C. performed *in situ* transport measurements. D.P. and K.I.B. participated in sample preparation. D.C. and A.B. provided the bulk $MoSe_2$ sample. N.J.G., J.Y. and D.G.M. provided the bulk $MoSe_2$ and WSe_2 samples. N.T.C., M.O. and S.O. contributed to DFT calculations. W.Z., J.C.I. and A.R.L. participated in STEM experiments. W.Z., K.S., S.J.P. and S.T.P. supervised the project. J.L., O.C. and W.Z. wrote the manuscript, with advice from K.S., S.J.P. and S.T.P. This work was performed in partial fulfilment of the requirements for a PhD degree by J.L.

Additional information

Supplementary information is available in the online version of the paper. Reprints and permissions information is available online at www.nature.com/reprints. Correspondence and requests for materials should be addressed to J.L. and W.Z.

Competing financial interests

The authors declare no competing financial interests.